Coevolving edge rounding and shape of glacial erratics; the case of Shap granite, UK

Paul A. Carling[1]

[1]School of Geography and Environmental Science, University of Southampton, Southampton, SO17 1BJ, UK

Correspondence to: Paul A. Carling (p.a.carling@soton.ac.uk)

Abstract

The size distributions and the shapes of detrital rock clasts can shed light on the environmental history of the clast assemblages and the processes responsible for clast comminution. For example, mechanical fracture due to the stresses imposed on a basal rock surface by a body of flowing glacial ice releases initial 'parent' shapes of large blocks of rock from outcrop, which then are modified by the mechanics of abrasion and fracture during subglacial transport. The latter processes produce subsequent generations of shapes, possibly distinct in form from the parent blocks. Lacking is a complete understanding of both the processes responsible for block shape changes and the trends in shape adjustment with time and distance away from the source outcrop. Field data on edge rounding and shape changes of Shap granite blocks (dispersed by Devensian ice eastwards from outcrop) are used herein to explore the systematic changes in block form with distance from the outcrop.

The degree of edge rounding for individual blocks increases in a punctuated fashion with the distance from the outcrop as blocks fracture repeatedly to introduce new fresh unrounded edges. In contrast, block shape is conservative, with parent blocks fracturing to produce self-similar 'child' shapes with distance. Measured block shapes evolve in accord with two well-known models for block fracture mechanics — 1) stochastic and 2) silver ratio models — towards one or other of these two attractor states. Progressive reduction in block size, in accord with fracture mechanics, reflects the fact that most blocks were transported at the sole of the ice mass and were subject to the compressive and tensile forces of the ice acting on the stoss surfaces of blocks lying against a bedrock or till surface. The interpretations might apply to a range of homogeneous hard rock lithologies.

Short Summary

Edge rounding in Shap granite glacial transported boulders is an irregular function of distance from the source outcrop in northern England, UK. Block shape is conservative, evolving according to block fracture mechanics — stochastic and silver ratio models — towards either of two attractor states. Progressive reduction in size occurs to blocks transported at the sole of the ice mass where the blocks are subject to the compressive and tensile forces of the ice acting against a bedrock or till surface.

Key words

Glacial erratics, erratic rounding, erratic shape, fracture, subglacial

1 Introduction

The concentration, size, shape, and the degree of rounding of glacial ice-transported blocks of rock may change with distance from the source outcrop. Spatial trends in concentration have been used frequently to indicate preferred ice flow directions (Kujansuu and Saarnisto, 1990; Evans, 2007, Benn and Evans, 2011, p. 675). Concentrated bands of ice-freighted erratics are referred to as 'indicator plumes', 'indicator trains' or 'indicator fans', with concentrations dropping off rapidly outside of the plumes due to ice-flow induced dispersion (Larson and Mooers, 2004). None-the-less, concentration is also sustained by comminution, whereby blocks fracture, or abrade to form smaller blocks and fragments through time and distance from the source outcrop. In contrast to dispersion, there has been less focus on changes in size, shape, and edge-rounding with distance from source (Benn and Evans, 2011). The changes in the shape of blocks are functions of the mechanical properties of the blocks, primarily rock strength and structure, as well as the physical processes promoting comminution. A change in block shape also represents a change in block size. To explore the controls on edge rounding and the shape of erratics, dispersal from a well-known exposure of the Shap granite (Sg) in the UK was examined in the present study. Improved understanding of process controls related to edge rounding and fracture should shed light on the associated basal ice dynamics related to block form changes generally. The two key issues are: 1) the relative importance of fracture mechanics in reducing block size in contrast to edge-rounding and 2) whether edge-rounding and shape coevolve with distance from the source outcrop.

1.1 The Study Area and Context of the Study

The exposure of the Sg pluton occupies a small area (*c.*, 7 km^2) in the eastern English Lake District (Fig. 1) defining a distinct, small, source area for granite blocks. The variation in the concentrations of Sg blocks with distance from the pluton has been used as a key indicator of the directions of ice

movement across northern England (reviewed by Carling *et al*., 2013) during the Dimlington Stadial (*c*., 29 ka BP to 14.7 ka BP) within the Last Glacial Period (*c*., 115 ka BP to 11.7 ka BP; Rose, 1985; Scourse et al., 2009; Chiverrell and Thomas, 2010; Davies et al., 2019; Clark et al., 2022). Around the Last Glacial Maximum (LGM: 26.5 ka BP to 19 ka BP, Clark *et al*., 2009), the region was covered by ice, several hundred metres thick (Evans *et al*., 2009), and Sg blocks were entrained from the subglacial bedrock (Ugelgiv *et al*., 2016). Long Fell, on the eastern margin of the exposed pluton, is a kilometre-scale rôche moutonnée, severely ice-plucked in the east and south-east at Wasdale Crag (Fig. 1), with smooth, ice-planed surfaces occurring to the north, west and on the summit (point 452 m above sea level), indicating the erosional effects of moving ice and debris (Hallet, 1981). The west to east change in the style of erosion, from smoothing to plucking, is consistent with ice in the vicinity of the pluton moving predominately to the east in an early phase (*c*., 29-25 ka BP; Livingstone *et al*., 2012; Merritt *et al*., 2019) of the Dimlington Stadial, and generally northwards across the pluton subsequent to 22 ka BP, *i.e.* towards the end of the LGM (Livingstone *et al*., 2012; Merritt *et al*., 2019); the latter supposition consistent with the W.S.W. to E.N.E. orientation of glacial striations on the pluton (Nicholson, 1868).

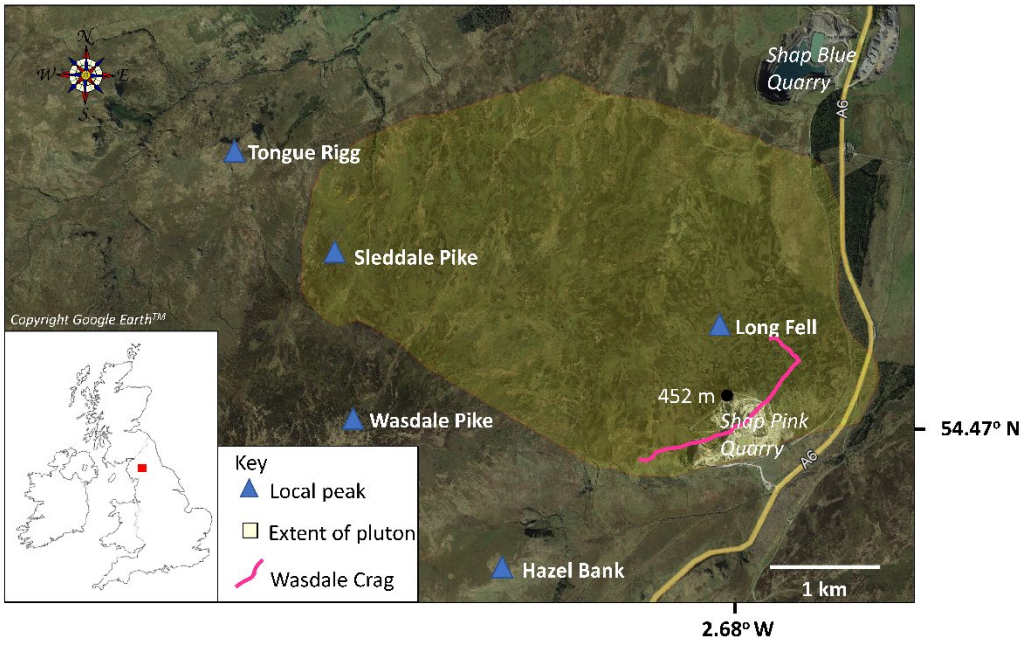

Figure 1: Location of the Shap granite pluton relative to the A6 highway. The central portion of the ice-plucked outcrop (Wasdale Crag) crag has been destroyed by quarrying. Spot height elevation is metres above sea level. Base map is from Google Earth™. Approximate extent of the Shap Granite pluton outcrop from the British Geological Survey (https://www.bgs.ac.uk/map-viewers/geoindex-onshore/).

In terms of concentration, the dominant dispersal of Sg erratics, during the early phase of the Dimlington Stadial (Stage I; *c*., 29-25 ka BP; Merritt *et al*., 2019) was eastward (Carling *et al*., 2013) within sustained ice flow through the topographically controlled corridor of the Stainmore gap across the North Pennines hills (Fig. 2A). The plume extended as far as the east coast of England; a distance more than 100 km (Fig. 3). Block size tends to diminish with distance, although examples of far-travelled large blocks occur sparingly (Carling *et al*., 2023). Due to shifting ice divides and competing ice dispersal centres (Evans *et al*., 2009; Merritt *et al*., 2019), subsequently two Sg plumes dispersed in southerly directions until, in the late stadial, erratics briefly were dispersed northwards from the vicinity of the pluton (Carling *et al*., 2013) in accord with the ice movements reported by Livingstone *et al*. (2012). These latter dispersal directions are not considered further herein. The focus solely is on those erratics the final transport vectors (direction and distance) which are roughly due east, defining a simple linear direction over which changes in the nature of the erratic populations might be measured.

Less well understood than directions of travel and changes in concentration, is the process of edge-rounding and shape changes of Sg blocks that accompany size reduction. The granite is an ideal choice for study as the composition and texture is uniform (Grantham, 1928), mostly giving a massive, unlayered, structure to individual blocks. Layering, such as found within sedimentary rocks, would add complexity to the study of shape evolution, which is avoided in this study. Hopkins (1849) had commented briefly on the rounding of Sg blocks (density ~ 2.61 tonnes m^{-3}) as size reduces towards the east coast, yet such rapid changes in form are seemingly at odds with the high strength of the rock. The strength of Sg in compression exceeds 207 MPa (Holland, 1959;

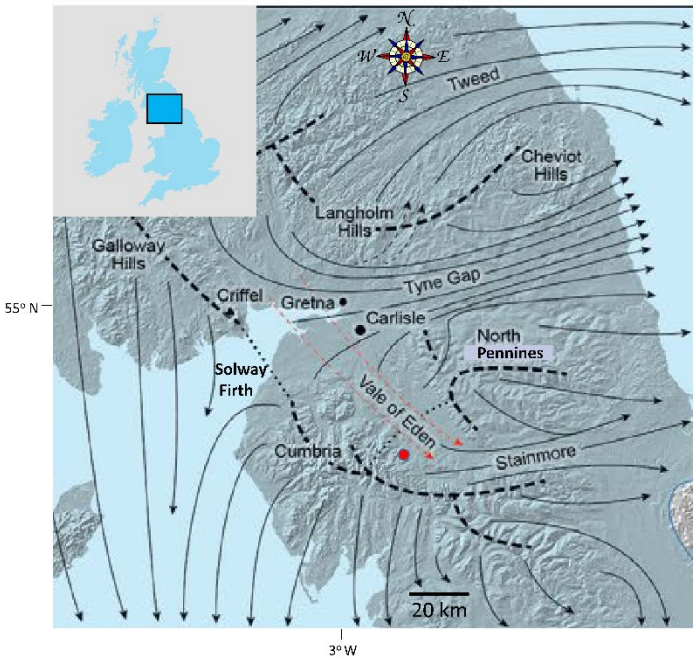

Figure 2: Ice flow directions for Stage I (29-25 ka BP) of the last British-Irish Ice Sheet around the Solway Firth (from Merritt et al., 2019. Reproduced with permission) in northern England (inset panel). Eastward ice flow through prominent topographic corridors occurs across the North Pennines. Broken and dotted black lines refer to ice divides. Black arrows indicate ice-flow vectors (dotted redarrows indicate alternative ice-flow scenarios). Topography from NEXTMap digital elevation data. Shap granite erratic plume dispersed to the east from the pluton (red dot) chiefly over Stainmore (see Fig 3).

Day and Goudie, 1977; Goudie, 2006) such that the rock is considered 'very strong' (British Standards, 1981). Despite the rock strength, Hodgson (1870) had remarked on how seemingly rapid rounding of granite might be aided by rock friability due to a high mica content associated primarily with biotite (Firman, 1953). Biotite is soft compared with the large phenocrysts of feldspars and quartz (Firman, 1953) that dominate the granite composition. Nevertheless, there has been no investigation of the changes in shape and rounding of Sg blocks with distance from the source; with very few granite blocks visually maintaining significant mass over tens of km. A study of blocks exposed on the modern land surface, away from major watercourses, should reveal rock-wear processes associated with glacial transport as there has been negligible losses to Sg surfaces due to post-glacial subaerial weathering (Wager, 1944; Parsons and Lee, 2005). The few weathered examples of blocks exhibit phenocrysts standing proud (3-5 mm) of the matrix, as the mica is readily subject to chemical weathering if *buried*

but the feldspars are not much altered (Wager, 1944). Consequently, an hypothesis was proposed: '*Sg ice-transported blocks would display systematic changes in edge-rounding and shape'*; with an aim *'to demonstrate if edge rounding and shape coevolve with distance to the east from the pluton'.*

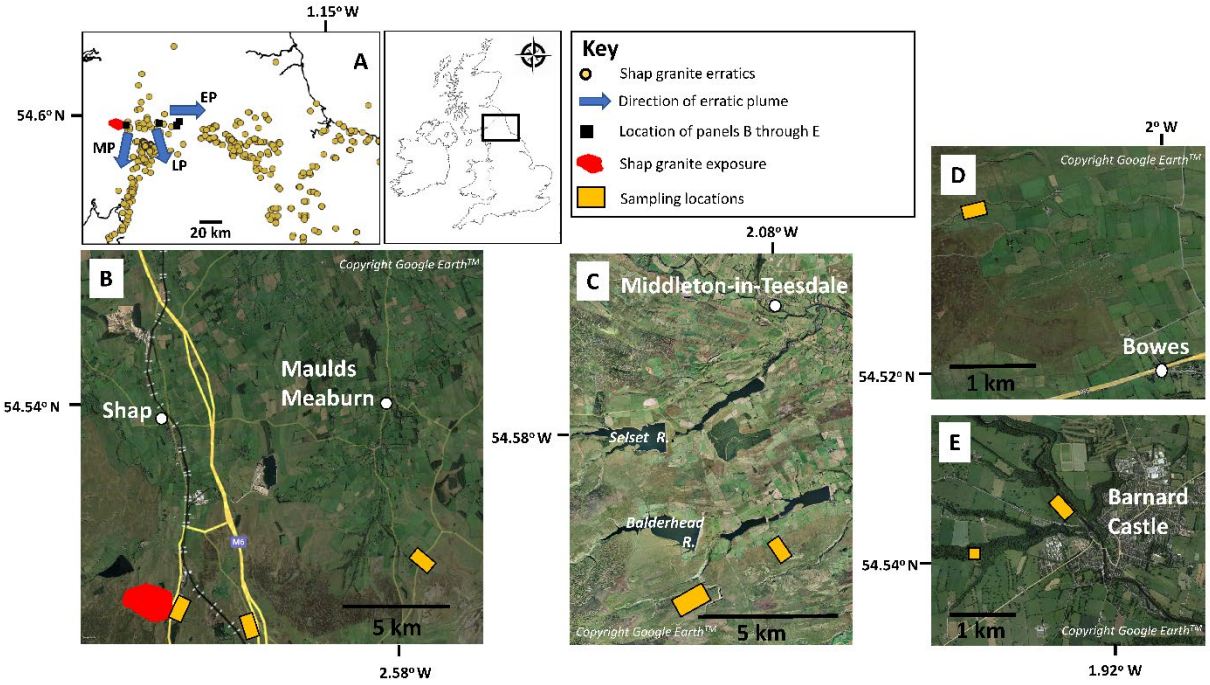

Figure 3: A) Spatial distribution of examples of Shap granite erratics within the study area, northern England (inset), showing the early easterly-directed plume (EP) and the later southerly Mint and Lune plumes (MP and LP) relative to the source outcrop of Shap granite. Locations shown within panel A are indicative of the general sampling areas of: B) Wasdale Bridge, Haybanks, Blasterfield; C) upper Teesdale; D) Levy Pool; E) Barnard Castle. See main text for details. Base maps copyright Google Earth™.

Shape (and size) changes in a Shap granite block occur due to three predominant processes which scale from affecting small areas of a block to larger areas:

1) abrasion, whereby grain-size fragments (*e.g.,* phenocrysts) are ground-off the block surface (Haldorsen, 1981; Benn and Evans, 2011) primarily by shear stresses associated with blocks moving across a bedrock or till surface in the direction of basal ice motion, or by ice and till moving over stationary blocks lodged against the substratum - this process can result in distinct rounded surfaces on a block (Boulton, 1978; Hallet, 1979);

2) spallation, whereby flakes of rock are freed from the surface of the block (Olsen, 1983) due to externally-derived and internally-derived tensile deviatoric stresses in the rock, both imposed by the motion of the ice overburden, with the shear stresses acting on planes at less than the block scale (Li *et al*., 2018) – this process reduces block mass but results in localized scarred surfaces;

3) fracture (Buscarnera and Einav, 2021) whereby the 'parent' block splits into substantial parts (often two; here referred to as 'child' products). The propagating fissure ultimately may be due to compression loading but, at the block surface, it is the result of a tensile stress (acting on a plane at block scale) flexing the stoss surface of a brittle block lying on a hard basal surface, leading to fissure development often transverse to the direction of basal ice motion (Morland and Boulton, 1975; Hallet, 1996; Benn and Evans, 2011, p. 264). The tensile strength of a rock is typically an order of magnitude less than the compressive strength (Li *et al*., 2018). This tripartite classification informed the Method.

To address the hypothesis, the focus of the study is abrasion and fracture, but observations on spallation were obtained for completeness, with the latter results reported within Supplementary Information section 2.1. There is justification from studies of bedrock outcrop erosion by basal ice that both the degree of abrasion of bedrock surfaces and the number of fracture events are related to time in transport (Cohen *et al*., 2006) and thus the distance erratics are moved.

2 Method

Shap granite blocks were sampled along a west to east transect, starting from below Wasdale Crag. It was assumed that all the sampled blocks were from the same population subject to basal traction transport (*vis*. Boulton, 1978) for much of the transport histories; the population being a coarser

component of a subglacial traction till (*sensu* Evans *et al*., 2006) deposited during the waning of the easterly phase of ice motion (Fig. 3A) (Hallet, 1979). Blocks ($L > c.$, 1.0 m) were located by field walking. Locations sampled include Wasdale Old Bridge, Haybanks, Blasterfield, sites near Barnard Castle in Teesdale and Levy Pool near Brough (Table S1), respectively 0.8 km, 3.5 km, 8.4 km, *c*., 36 km and *c*., 41 km from the Wasdale Crag outcrop (Fig. 3). From preliminary site survey, the sites selected were known to have sufficient erratics within defined areas for sampling. However, to obtain similar sample sizes, the areas searched for the final two locations necessarily increased as the surface density of blocks decreased eastwards. Examples of erratics were selected that were sitting on exposed bedrock or till surfaces, so as not to be partially buried. Distance from the source outcrop is assumed to relate to time in transport.

At each location, edge, and shape measurements and scar enumeration were made on thirty blocks as briefly described below; the full procedure developed within Supplementary Information. The sample size was found to be sufficient (Daniel, 1999; Conroy, 2018) for the aims of the project and, moreover, interpretation of data trends became possible once the sample size, *n,* reached 30 at each location. These data were supplemented by a regional shape data compendium (Carling *et al*., 2013). Changes in block size with distance from the pluton are not considered herein using field data, as a statistically significant sample size at each location would have to be prohibitively large to reflect the complete size range of blocks. Rather block size changes are considered within a theoretical framework related to shape changes. Blocks are considered as cuboids consisting of *faces* and *edges*.

In accord with 1) abrasion: edge rounding was measured after Wentworth (1923; Kirkbride, 1985). In brief, each of the three most tightly rounded edges on the visible portion of each block was defined by a chord (l), delimiting a segment of the block beneath each rounded edge, to give between 80 and 90 values for each location. Consideration of the height (h) of the segment in relation to the chord length constrains the radius (r_c) of an inscribed circle beneath the rounded edge (see Fig. S2 in Supplementary Information section 1.4), which radius is a measure of the degree of rounding:

$$r_c = \frac{l^2}{8h} + \frac{h}{2} \quad (1)$$

The radius of curvature reduces as the chord length reduces towards zero and often a right-angle corner occurs when r_c approaches 0. More rounded blocks have larger radii of curvature than less rounded blocks as the sizes of the inscribed circles increase as edges become less sharp. In similar fashion, the edge rounding was measured for joints bounding *in situ* Shap granite blocks constituting the outcrop of Wasdale Crag. These latter data provide a base line of the degree of edge rounding of blocks which have been subject to ice abrasion in place, but without subsequent transport.

To consider 3) shape changes by fracture: from initial field reconnaissance, blocks close to the source often appear cubic, but polyhedrons occur sparingly - ranging from wedges to prismatoids. Further from the source more ellipsoidal forms are evident. Consequently, to obtain an indication of the shape of a cuboid or an ellipsoid block (Fig. S1), the lengths of the three orthogonal axes: long axis (*L*); medium axis (*M*) and the short axis (*S*) were recorded in the field – polyhedrons were not sampled – to give *c.*, 30 values for each location. Consideration of the mechanics of shape changes also sheds light on the size reduction process with distance. Fracture within individual blocks is sometimes associated with joints and other block-scale planes of weakness. Yet, ice compressive force is the predominant mechanism for significant progressive change in shape for homogeneous granite blocks, inducing tensile fracture and block size reduction. Shape and size changes were examined either via a stochastic fracture model, applicable to fracture at right-angles to either of the *L*, *M* or *S* axes (Domokos *et al.*, 2015) of ellipsoidal blocks or, in accord with the silver ratio model applicable to cuboid blocks fracturing across the *M*-axis alone (Buscarnera and Einav, 2021), as is explained in the Results. Shape indices are reported in the main text using the Zingg (1935) projection, whilst an example of a simple ternary diagram (Fig. S3, after Hofmann, 1994) is provided in Supplementary Information section 1.5.

3 Results

3.1 Edge rounding

As is evident from the form of equation 1, rounding is a positive function of the square of the length of the chord of the segment, l, and an inverse function of the segment height, h (Fig. 4). As the inscribed radius values are obtained from both the values of l and h (Equation 1), there is an element of co-variance between the two axes in both panels A and B of Fig. 4. However, plotting the data in this manner allows ready visualization of the trends of the radius data (r_c) relative to the variation in the controlling parameters (l,h). Lower limits to data plotting positions occur in both panels equal to: $r_c = l/2$ and $r_c = h$ respectively.

The joint rounding on the pluton is less developed in comparison with the rounding of edges of blocks only 0.8 km away at Wasdale Old Bridge (Fig. 4). Although the range in heights of the segments are similar for both locations, the range in chord lengths for the pluton includes smaller values giving overall 'sharper' edge profiles for the pluton joints in contrast to the Wasdale Old Bridge blocks. It is evident that any 'parent' blocks newly entrained from the outcrop will exhibit both lightly rounded joint edges (glacially abraded when *in situ*) as well as sharp, fresh edges, the latter due to fracture upon release from the outcrop. However, although the initial lightly rounded edges can be further rounded with distance, fracture of entrained blocks introduces new 'sharp' edges as detailed next.

Although as distance increases larger radii are more frequent, small radii also occur at distance (Fig. 4). It is unlikely that small radii can survive abrasive transport over several tens of km from the pluton, rather repeated fracture introduces new sharp edges and thus new small radii to different generations of blocks. These new sharp edges begin to round far from the pluton. Although the plots of Fig. 4 are developed considering singular data points from many blocks, if the trends are considered to represent the rounding evolution that would occur for individual blocks, then the black arrows indicate the general direction of edge rounding evolution (*i.e.,* Fig. 4 panel A: if *h* is constant and *l* is variable;

panel B: if *l* is constant and *h* is variable). The linear functions in Fig. 4B allow ready comparison between locations such that, for any value of *h*, the degree of edge rounding is more pronounced with distance from the pluton; specifically, the linear curves (green, blue, purple, and red) have increasing values of the constant (*i.e.*, 1.71, 4.37, 4.69; 5.53 respectively). Similar linear functions for values of *l* can be applied to Fig. 4A but, for the sake of clarity, these curves are not plotted. The detail of edge

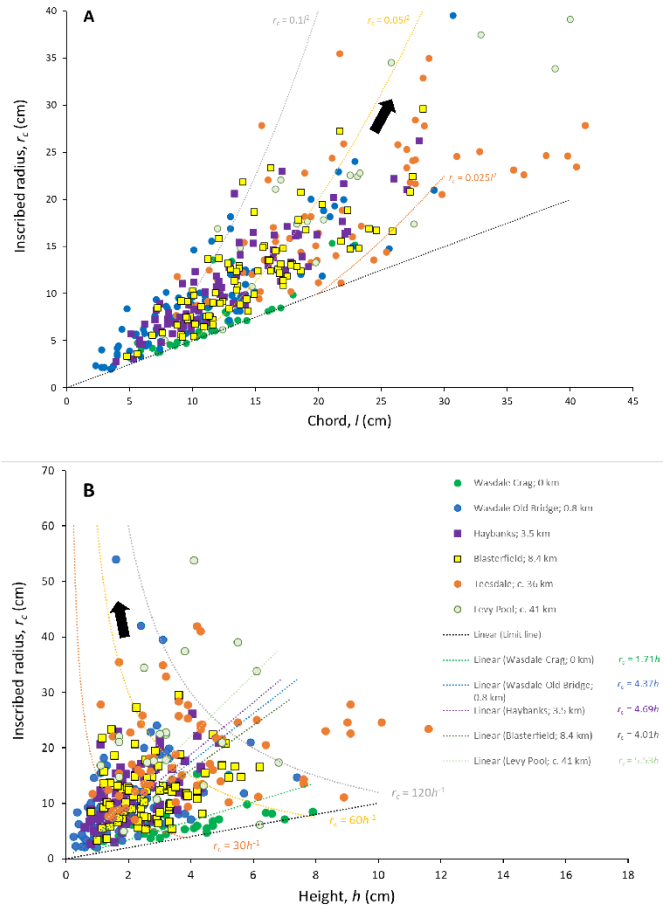

Figure 4: Trends in the values of the inscribed radius as a function of: A) chord length, and B) segment height. Black arrows indicate the direction of travel of the hypothetical function for an individual block (see main text). Examples of hypothetical curves (brown, yellow and grey) for the trends in individual clast evolution are given for both $r_c \propto l^2$ *and* $r_c \propto h^{-1}$. *Key to symbols in panel B also applies to panel A.*

rounding is considered within the Discussion, as edge-rounding of individual blocks is not a smooth function of distance from the source as might be inferred from the black arrows in Fig. 4 and from

mean radius of edge rounding with distance from the outcrop (Fig. 5). The latter figure depicts an exponential increase in the mean radius of curvature with distance (D_s) from the source outcrop:

$$r_c = 10.3881e^{(0.0194D_s)}. \quad (2)$$

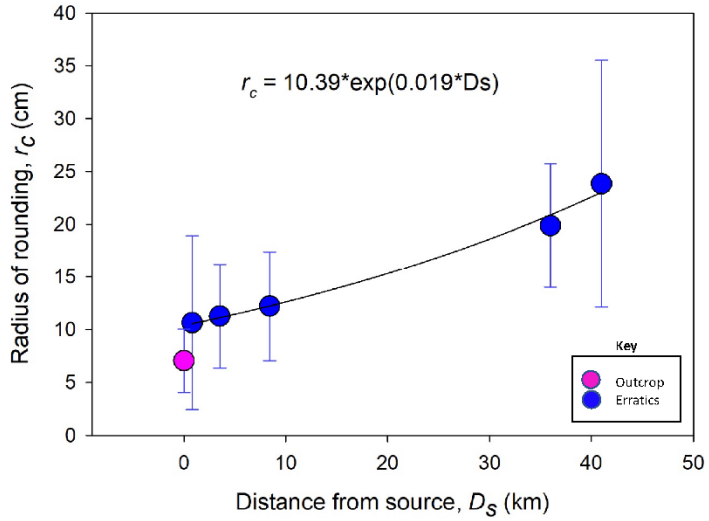

Figure 5: Mean values and s.d. of edge rounding as a function of distance from outcrop.

3.2 Shape evolution

In the context of natural hexahedrons, the *stochastic model* of progressive fracture due to the stress of compression (Domokos *et al*., 2015), describes the generation of ellipsoids with the orthogonal axes length proportions: 2.32; 1.52: 1 (Fig. 6A), whereas the *silver ratio* progressive fracture model (Buscarnera and Einav, 2021) describes the generation of cuboids with the edge length proportions: $\sqrt[3]{2^2}$; $\sqrt[3]{2}$; 1, *i.e*.; 1.59: 1.26: 1 (Fig. 7A). In the former model, a fracture plane is orthogonal to any of the three sides of a cuboid (enclosing the ellipsoid) and separates two pieces of equal mass. In the silver ratio model, a fracture plane occurs orthogonal to the current longest axis, separating two pieces of equal mass. In nature, deviation from these two models can occur such that shape self-similarity, in terms of axial ratios, is not maintained necessarily upon successive fracture events if the subsequent fracture is across an axis that differs from the previous fracture event. Fracture across the plane of

the short axis was observed in nature (Fig. 6B). However, systematic fracture across the plane of the long axis (Fig. 6C) and across the medium axis (Figs. 6D, 7B) appeared predominant (*vis* Benn, 1992) for the blocks observed in the field, in accord with both the stochastic and silver models. Given that most blocks rest with the short axis vertical, fracture across the *L* or *M* axes is consistent with known fracture mechanics, whereby the centre of an object is the location, under loading, of the maximum in the tensile stress and the consequent nucleation point for fracture (Hiramatsu and Oka, 1966; Shipway and Hutchings, 1993). From this point, a fracture line develops to the block edges (Man *et al.,* 2018) transverse to the direction of tensile loading. For low values of static or dynamic loading, the rock eventually ruptures into two parts (Man *et al*., 2018). Thus, although a block on occasion might fracture across an axis at variance with the two models above, there is a tendency for blocks to evolve towards one or the other model. The system state attractors for these two models are shown in Fig. 8, wherein natural block shapes are considered. Importantly, compression and tensile fracture leads in both models initially to uniquely defined anisotropic forms, although isotropic forms (*L* = *M* = *S*) can occur in principle with progressive fracture if the fracture rule in each model is relaxed and varied.

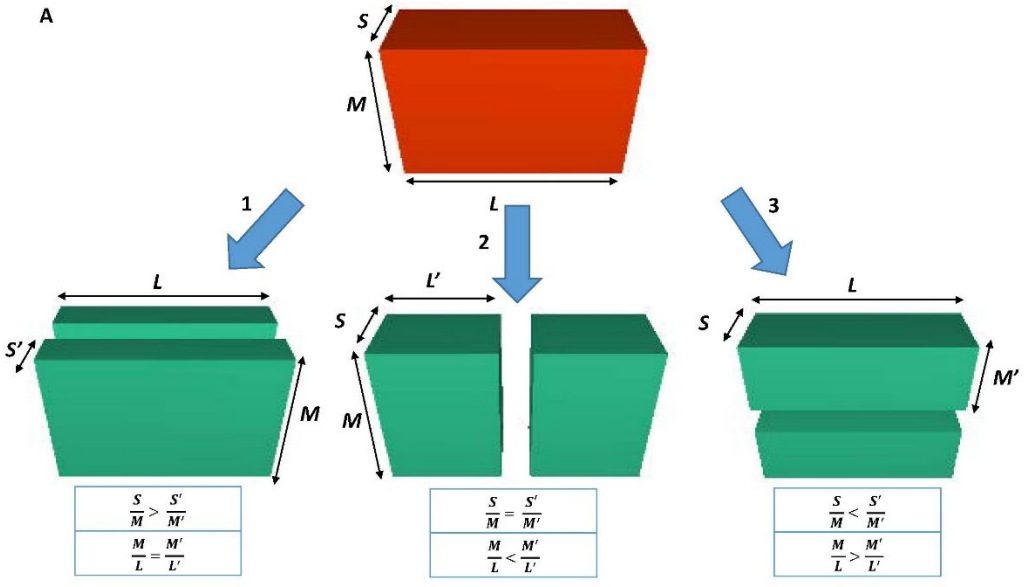

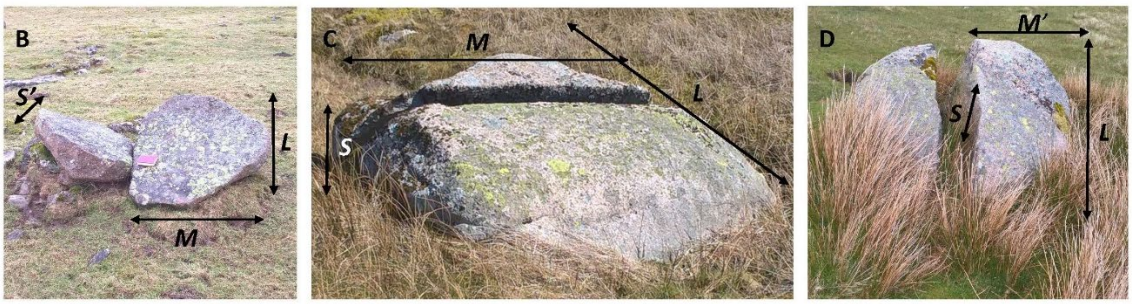

309

310 *Figure 6: A) Schematic representation of the concept of the stochastic fracture model applied to a*
311 *three-dimensional cuboid (enclosing an ellipsoid – see Fig. S1) subject to successive fracture given an*
312 *assumed identical stress loading to the granite block at each fracture event. Fracture planes are*
313 *orthogonal to a side and separate two pieces of equal mass. Shape self-similarity is not maintained*
314 *upon successive fracture events. Three different fracture styles are possible within the model, as*
315 *labelled 1, 2 and 3; B) Example of a well-rounded block split along a fracture plane consistent with*
316 *model 1; C) Example of a well-rounded block split along a fracture plane consistent with model 2; D)*
317 *Example of a well-rounded block split along a fracture plane consistent with model 3. The long axes*
318 *are foreshortened in panels B, C and D.*

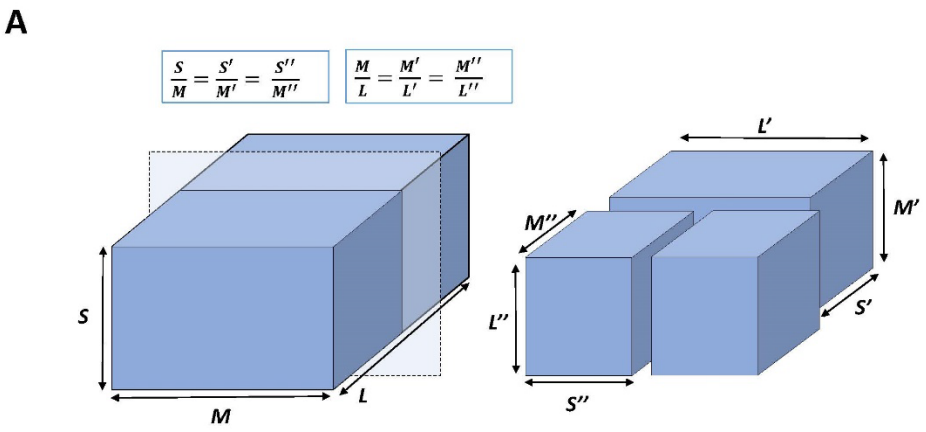

319

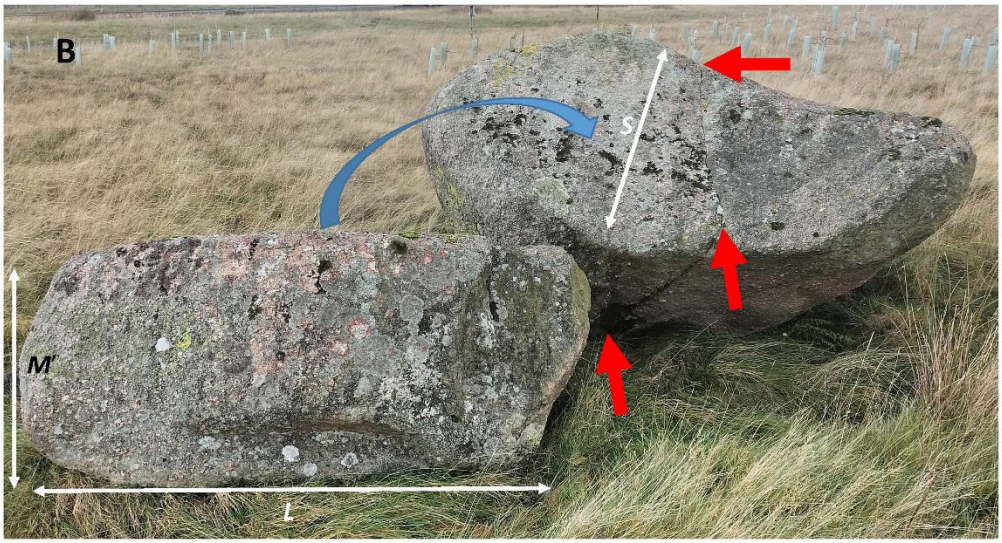

Figure 7: A) Schematic representation of the concept of the silver ratio model applied to a three-dimensional cuboid (– see Fig. S1) subject to successive fracture given an assumed identical direction of stress loading to the granite block at each fracture event. Fracture planes are orthogonal to the current long axis. Shape self-similarity is more closely maintained (in contrast to Fig. 6) upon successive fracture events; B) Example of silver ratio block. Block to left is approximately the same size as the block to the right and the lower surface (not seen) was originally on the top surface of the right-hand block with the exposed failure plane bisecting the M-axis alignment of the original parent block. The red arrows delineate a fracture plane, aligned with the M-axis of the right-hand block, which divides the right-hand block into two near-equal halves.

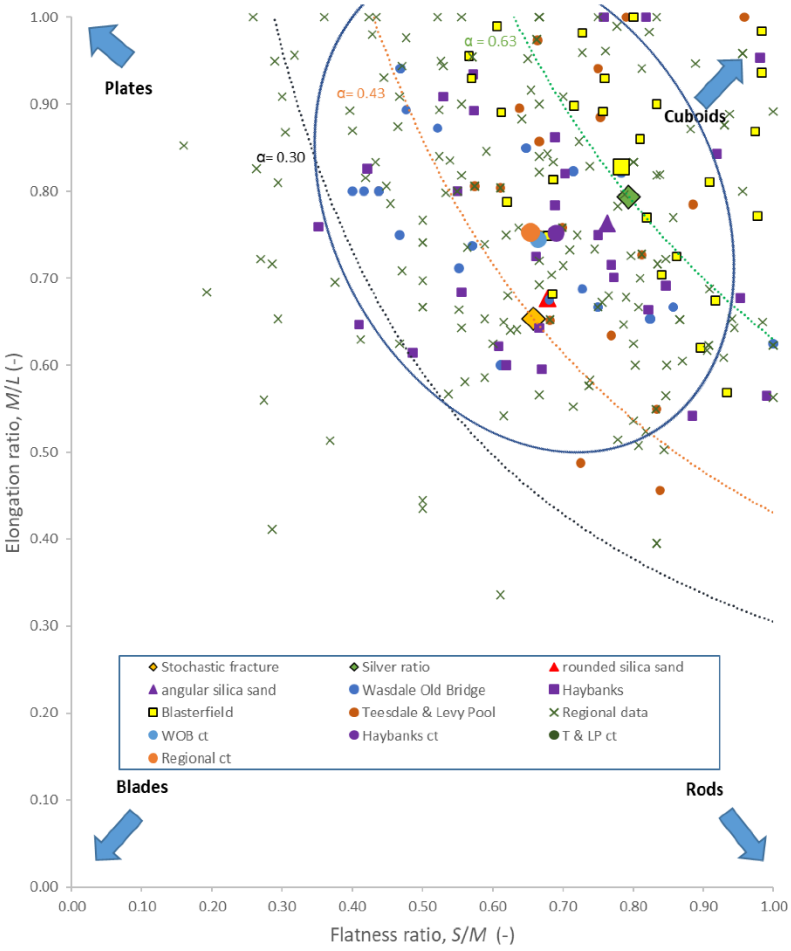

331

332 *Figure 8: The shape relationship for blocks in terms of the Zingg (1935) ratios. The system state*
333 *attractors for stochastic fracture (gold diamond) and silver ratio (green diamond) are shown as*
334 *larger symbols, as are the central tendency shapes for mechanically crushed silica sand grains that*
335 *were initial sub-rounded or angular (Seo et al., 2021). The central tendency (ct) for each sampled*
336 *location, defined by the mean values, are shown as larger symbols. Curves represent the trend in*
337 *values of M/L and S/M for constant values of S/L. ct symbols represent the central tendency of each*
338 *population. Oval is the 95% contour after Oakey et al. (2005).*

339

340 Within Fig. 8, the Zingg ratios (*S/M and M/L*) for the sampled locations are plotted together with a
341 data set for the broader region (Regional data). Within Fig. 8, completely equant (isotropic) forms
342 are absent and plate-like forms survive more readily than rods. Nonetheless, the central tendency of
343 block shape within the regional data is *S/M* = 0.65 and *M/L* = 0.75; *i.e.*, roughly midway between the
344 system state attractor for stochastic fracture and the silver ratio attractor. Lines of constant equal
345 aspect ratios (*S/L*) are shown for the silver ratio model (α = 0.63) and for the stochastic fracture model
346 (α = 0.43). Seo *et al*. (2021) showed that for homogeneous silica grains, fracture depended on initial

particle form (Fig. 8) with angular grains tending towards the silver ratio whilst rounded grains tended towards stochastic fracture. If the fracture process is scale-invariant, then the size differences between silica grains and the Shap blocks can be ignored, and one would expect the Shap granite (a largely homogeneous lithology) to migrate across the diagram from silver to stochastic fracture as cubic blocks become progressively more rounded and ellipsoidal. Blocks deviating from either model (either too long or flat, *e.g.*, approaching $\alpha = 0.30$), will tend to fracture and migrate back towards $\alpha = 0.43$, as is especially evident in Fig. S6B within Supplementary Information section 2.2. The central tendencies of the regional data and each of the sampled locations are closely grouped between the central tendencies of the silver and stochastic fracture. The exception is the Blasterfield location which lies closer to the silver ratio, but with increased distance of transport, Teesdale and Levy Pool blocks are in accord with stochastic fracture. Thus, it is evident that block fracture fluctuates between each model, with a trend for constant equal aspect ratios close to $\alpha = 0.50$ (not plotted in Fig. 8).

Although Fig. 8 provides an impression of the spread of block shapes around a central tendency there is no clear impression of the actual shape evolution as possible representative shapes can only be selected arbitrarily from the data clouds. Further, only the cube (or sphere) limit point (*e.g.*, 1, 1 in Fig. 8) is real. Limit points for rods and plates exist only through mathematical definition, because as the rod and plate limit points are approached, rods become infinitely long and plates infinitely thin. Thus, representative shapes need to be selected objectively. To solve this problem the procedure of Oakey *et al*. (2005) was utilized to define representative shapes that define the 95% contour around the central tendency of the regional data, represented by the blue oval in Fig. 8. With reference to the position of the 95% contour in the blade quadrant, curve $\alpha = 0.30$ is selected to demarcate a lower bound for common block ratios; with a few plate-like or rod-like blocks occurring in the lower portion of the diagram.

3.3 Size evolution

The size distribution of the Shap granite blocks with distance from the pluton source has not received detailed attention, although Carling *et al*. (2013) provide some general observations suggesting there is size reduction with distance. In this study, the sample sizes were insufficient to demonstrate the reduction in block size expected with distance from the source outcrop. However, controls on size reduction are evident. Specifically, blocks greater than L = 4 m are rare (Carling *et al*., 2013), the size being controlled by the close joint spacing of the granite at source (Firman, 1953). With few exceptions, large blocks (L > 3.0 m) do not occur beyond 7 km from the pluton, at which point medium blocks (2.5 > L > 1.5 m) become scarce, with small blocks (1.5 > L > 0.5 m) and cobble-sized material dominating with further dispersal (Carling *et al*., 2013). These observations indicate that there was a control on the upper size of blocks entrained from the pluton and fracture rapidly reduced block size inducing a crude size-reduction down plume within just a few kilometres. This process was accompanied by local deposition of abrasion and spallation debris as components of a subglacial traction till. Nevertheless, the fracture mechanics that control block shape inevitably control size evolution (Figs. 6 and 7). For example, fracturing a parent cube with 4m long edges and its progeny across the L-axis, only six sequent fracture divisions are required to produce a 1 m cube, as will be demonstrated in the Discussion.

4 Discussion: The context of size and shape constraints

The initial hypothesis proposed that Sg ice-transported blocks would display changes in edge-rounding and shape with distance to the east from the pluton. As shown in the Results, and elaborated below, edge-rounding does change with distance but block shape is conservative.

Space-time substitution is an underlying tenant of this study, in that the size and shape characteristics of multiple individual blocks (an erratic plume), dispersing across the landscape, can reflect the

evolution of a single erratic block through time along the same general spatial trajectory. An adequate number of sampled blocks are required for this analogy to hold because perturbations to the population of erratics can occur during dispersal. For example, blocks can have been introduced to the W-E trajectory of the study plume by N-S ice movements reworking blocks previously deposited outside of the eastern-directed plume during periods of time after the main W-E ice flow. Also, for the purposes of determining transport distance, a zero *x*-axis origin has been assumed to be the most easterly outcrop of the pluton at Wasdale Crag. However, some blocks might have been sourced up to a few kilometres to the west of Wasdale Crag. Despite these potential perturbations, which include a small degree of subaerial weathering, the small sample sizes are sufficient to clearly demonstrate systematic change in edge rounding due to ice transport as well as block shape evolution. Finally, edge-rounding and shape are re-set to a degree for the children each time a parent block fractures, so the process of rounding and shape adjustment is not a smooth function of distance from the outcrop, as is explained below.

4.1 A conceptual model of block edge rounding controls

It should be acknowledged that this study has not considered abrasion of the faces of blocks but has focussed on the edges which tend to abrade and round more rapidly than the associated faces (Boulton, 1974). The edges of blocks still within the outcrop are sharp, albeit some are subject to a slight degree of rounding in place (Fig. 4) from glacial wear, as well as a little post-glacial subaerial weathering. Detached blocks close to the outcrop also tend to exhibit slightly ice-rounded edges, with sharply angled joint planes characterising the other faces due to fracture release of the block from outcrop. The increase in edge rounding with distance confirms the initial hypothesis.

Block edge rounding initially is constrained by the hardness of the Shap granite and the way it fractures when first entrained at outcrop. The absence of significant edge rounding at the outcrop indicates

423 that blocks were entrained continually until the imposed stresses fell below that required to quarry
424 further blocks. Otherwise, edge rounding of entrained blocks is associated with basal traction
425 transport (Boulton, 1978; Hallet, 1979). Although the compressive strength of granite is high, the
426 tensile strength is an order of magnitude lower; possible as low as 4% of the compressive strength,
427 *i.e.,* 8 MPa (Anikoh *et al*., 2015; Demirdag *et al*., 2018; Engineering ToolBox, 2008; Yu *et al*., 2018).
428 Thus, where compression is translated into flexure, the propensity of the block to elongate across the
429 axis of flexure leads readily to fracture of the brittle granite. This condition means that many blocks
430 close to source initially exhibited near right-angle edges (Fig. 4). Given this geometric constraint, radii
431 of edge curvature inevitable are small initially, approaching the limit: $r_c = l/2$ and $r_c = h$, and
432 increase with distance from the outcrop due to abrasion. However, fracture away from the outcrop
433 introduces new sharp edges (Figs. 4 and 8), such that larger radii characterizing an individual edge-
434 rounded block just before fracture are augmented by smaller radii. This change is reflected in the
435 scatter of radii values found with increased distance from the outcrop (Fig. 4). However, as block size
436 reduces, a condition is approached whereby the population of blocks are increasingly those which
437 resist fracturing (see section 'Block size controls') which should allow edge rounding to become more
438 persistent and thus more pronounced with distance. This condition may be approached in the case
439 of the examples from Teesdale (Fig. 4A) where it is evident that short chords become fewer with
440 distance as larger values of r_c begin to dominate the population. As blocks in transport can reorientate
441 within the ice flow, edge rounding has no effect on block shape, given the shape definition herein.
442 However, if blocks are not free to reorientate, a case not considered herein, the form of blocks can be
443 significantly affected by abrasion in place (Boulton 1974; Hallet, 1979).
444
445 Although a positive exponential function (Equation 2) describes the increase in the mean radius of
446 edge rounding with distance from the source outcrop (Fig. 5), the function must eventually transition
447 to a negative function as abraded smaller blocks inevitably are characterized by smaller radii of
448 curvature. This latter condition was not recorded within the current study and sampling at greater

449 distances from the source would be required to determine if this transition occurs. A block (*e.g.*, 1 m
450 cube) subject to edge rounding equally on all 12 edges, as per Equation 2, would have lost about 4%
451 of its mass after 10 km and 9% after 40 km so, in contrast, fracture into two self-similar parts whereby
452 50% of mass is lost, is more significant than edge-rounding in terms of mass loss per block. The greater
453 significance of fracture is consistent with studies of ice erosion by quarrying and ripping versus
454 abrasion of basal bedrock surfaces (see references in Cohen *et al*., 2006*;* Hall et al*.,* 2021).
455
456 Rounding of individual bocks is not a steady process, as is evident from the data scatter in Fig. 4 and
457 is further illustrated in the following section. The process whereby the percentage of edges of
458 different generations are rounding with distance, or time, is shown schematically in Fig 9A, wherein
459 there are initially no more than 12 slightly rounded edges to a cube block newly released from outcrop
460 (see Supplementary Information section 1.6 and Fig. S4 for detail of the model). The model is simple
461 but demonstrates the complexity in edge rounding that must accompany successive fracturing of
462 blocks. Fracturing the block successively across the *L*-axis introduces new generations of fracture
463 edges (sequent fractures – Fig. 9B) at the same time as reducing the number of edges on each new
464 block related to earlier fracture events (see Supplementary Information section 1.6 for further detail).
465 As the number of progeny blocks increases exponentially for each fracture event (Fig. 9C), and each
466 sibling can be further dissected along a choice of one, two or three *M*-axes depending on block shape,
467 a diagram including all fracture progeny introduces unreasonable complexity, obscuring the key
468 details. In Fig. 9A andB, for clarity, only one block is followed through one to six sequent fractures,
469 which reduces the number of data points for plotting to a manageable number. The key point to
470 illustrate is that the initial 'parent' block must be fractured five times for one of the ensuing progenies
471 to have lost all the initial 12 edges of the 'parent'. The total number of initial parent edges is relatively
472 persistent because there are 12 edges to begin with (Fig. 9). Contrarily, only four new edges (Fig. 9A)
473 per block are produced on each fracture event. Thus, in contrast to the curve for the initial parent
474 edges, the 1st fracture edges can be lost in as little as four fracture events depending on which sibling

block is considered. The 2nd fracture edges are lost by a total of five fracture events and so on, as more fractures occur adding new fracture edges. Relaxing the model to allow fracture across either the *M* or *S* axis (see Supplementary Information section 1.6) only adds one or two fracture events to the process of edge extinctions. Thus, by introducing new edges at each fracture event, rounding of the block with distance or time is not a steady progression, with well-rounded edges being lost as blocks are split at the same time as new immature edges are added to a population of sub-mature edges. The model may not apply beyond some undetermined number of fracture events if there is a critical minimum block size that is less susceptible to fracture (as was noted above) and rounding then can become pronounced. Nonetheless, this model explains the presence of a 'continuum' from well-rounded edges to less-well-rounded edges on many individual blocks. The issue as to whether there is a minimum block size is considered in the next section.

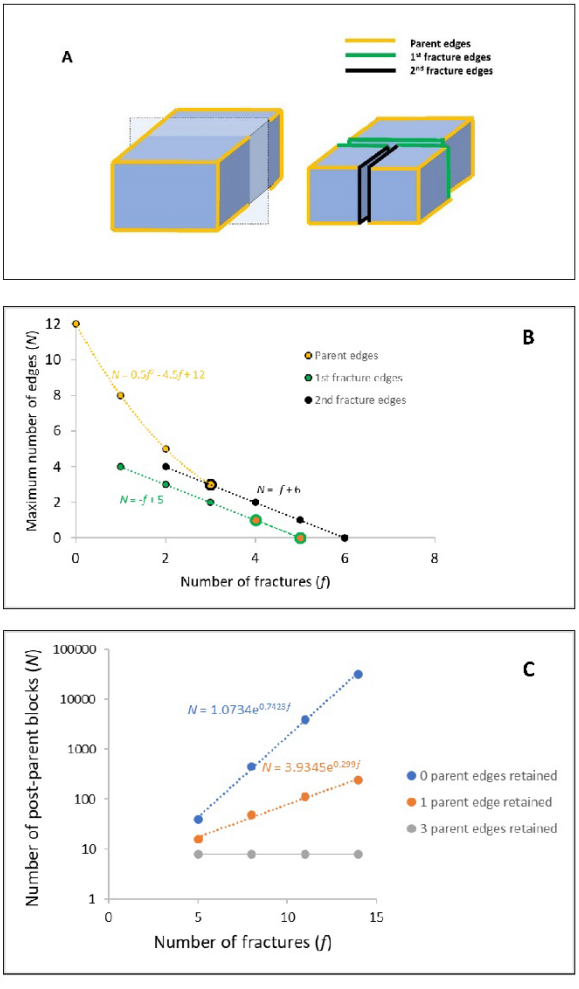

Figure 9: A) A regular block released from outcrop has 12 initial edges (Parent edges) all equally rounded. Fracturing the block at right angles introduces four new edges (1st fracture edges) to each of two sibling blocks, which edges are younger than the initial edges. A further fracture across the L-axis is indicated by 2nd fracture edges; B) The maximum number of edges of each generation on a block as a function of the number of fracture events, with only the parent edges and those edges related to the first two fracture events plotted; C) The total number of blocks created at each fracture event which retain 0, 1 or 3 of the original parent edges.

The significant increase in the mean radius of of edge rounding, with distance from outcrop (Fig. 5), indicates that the blocks were transported within a mobile concentration of basal debris, in frequent block-to-block contact and in contact with the bedrock, leading to abrasion before being deposited within a subglacial traction till (Hallet, 1979). If the distance travelled towards the east is not the controlling factor, then the high degree of edge-rounding may be due to prolonged temporal transport, with some material moving east, south, and then north again, extending the transport distances. However, compatible with studies showing block modification after distances of only 0.4 km (Humlum, 1985; Lliboutry 1994; MacGregor *et al.* 2009), an alternative main explanation is preferred for the easterly edge-rounding trend. Although Sg is mechanically strong in compression (Goudie, 2006) it is susceptible to abrasion and tensile fracture for the following reason. The blocks contain large pink phenocrysts set within a matrix of smaller mineral crystals. The large pink crystals are orthoclase feldspar (Moh hardness 6 – 6.5). The other common minerals are glassy quartz (Moh hardness 7), white plagioclase feldspar (Moh hardness 6) and black biotite mica (Moh hardness 2.5 – 3) (Caunt, 1986). Thus, the granular composition of the granite with harder crystals adjacent to a soft mineral may aid rapid rounding by abrasion and facilitate tensile facture during glacial transport.

4.2 Block shape controls

Block shape is dependent on the initial controls exhibited at: 1) the outcrop of origin; and 2) the subsequent transport history.

1) The primary control is the intersection of sub-vertical joints (Firman, 1953) in the granite with horizontal expansion joint planes caused by unloading (Jahns, 1943). Horizontal joints largely are due to glacio-isostatic rebound and surface erosion (Westaway, 2009), leading to the release of the residual stresses accumulated at depth (Berger and Pitcher, 1970). The resultant blocks initially tend to be cubic. Where blocks lie within a few metres from the parent outcrop, the block faces tend to be planar, although curved fractured surfaces occur occasionally, as do conchoidal fracture hollows on otherwise planar surfaces. Curved fracture surfaces tend to occur in homogeneous granite due to pressure unloading (Wang *et al*., 2022), which will have occurred as ice erosion reduced the overburden. Such joint-defined blocks within an outcrop are readily entrained by moving ice (Matthes, 1930; Morland and Boulton, 1975).

2) Although inhomogeneous blocks in traction may be envisaged as breaking down into multiple fragments at each compressive event (Boulton, 1978), the largely homogeneous nature of the Sg lithology leads to simple tensile fracturing, at each breakage event, whereby subsequent generations of blocks exhibit shapes largely similar to the parent forms. Thus, there is a tendency for equant blocks to persist, through time and distance, due to the tensile stresses associated with flexure across the stoss surfaces reducing block mass in accord with either the silver model or the stochastic model. This trend is indicated by the fact that stronger plate-like blocks occur less frequently away from the pluton in contrast to the general absence at distance of the weaker rod-like blocks. Thus, cuboids progress to form both cubes and cuboids such that the initial hypothesis is rejected.

4.3 Block size controls

Block size is dependent on the initial controls exhibited at: 1) the outcrop of origin; and 2) the subsequent transport history.

1) The primary control is the presence of the frequent, well-developed joint planes within the pluton (Firman, 1953; Caunt, 1986) which tend to define and delimit the range of the initial block sizes from *c*., 0.5 m to 4 m. Fault planes are of sufficient rarity to be ignored. Joints are largely orthogonal: *i.e*., sub-vertical and near horizontal but oblique joints also occur.

2) Once in ice-transport, other controls on block disintegration may pertain. In the present case, larger blocks close to the outcrop (< 0.8 km) often exhibit one (or more) intact or partially opened failure plane(s) inherited from the outcrop structure. More commonly, with distance from the outcrop (> 0.8 km), the planes of failure within individual blocks represent the directions of compressive and tensile forces exerted by the ice on the blocks (and thus bear no relationship to block structure or composition), as appears to be the case where failure planes are aligned with the *L* or *M* axes. Fracture occurred when the effective tensile stress exceeded the yield strength of the blocks. Glacial unloading, and subsequent stress release, also may introduce planes of weakness within transported blocks. Adopting the stochastic fracture mode or the silver ratio model for block shape changes indicates that block volume effectively halves at each fracture event with consequent reduction in block size. This conclusion has implications for the fractal evolution of erratic size distributions which, for brevity, cannot be addressed within this paper.

Other small-scale planes of weakness can be attributed to spatial variations in the primary mineral composition (Grantham, 1928; Parsons and Lee, 2005) leading to textural and grain-size variations which can be visible rarely as parallel lineaments, and later hydrothermal alteration also induced compositional and hence structural variations (Caunt, 1986). These weaknesses lead to loss of small blocks and flakes from the larger parent blocks (see Fig. S5 in Supplementary Information section 2.1) through spallation rather than fracture. Spallation may be related to the state of stress within a deforming till layer (LeBone Hooke and Iverson, 1995) rather than the tensile stress on the stoss side of a block which accounts for block fracture.

567

568 **4.4 General considerations**

569

570 A significant question is whether flowing ice can generate significant stress to fracture the granite
571 blocks. If the thickness of the deforming ice/till layer at the basal boundary is small relative to the size
572 of the boulder, then the compressive force is likely to dominate. However, if the converse applies
573 then the tensile force likely will dominate. Herein, given that there is no information as to the
574 thickness of the deforming layer, the distinction is not considered because, in most cases, blocks will
575 fracture at a lower stress due to tension in contrast to compression. In a consideration of similar
576 situations, emphasis was placed on the compressive strengths of blocks (Boulton, 1978) relative to the
577 normal stresses due to a static ice load above a block. In the present examples, the tensile strength
578 of the stoss side of a block resisting flexure is more relevant for brittle fracture and for granite can be
579 as low as 8 MPa, which is a tensile stress readily applied by a modest (*c*., 100m thick) yet dynamic ice
580 cover (Hallet, 1996). The distribution of compressive and tensile forces over the stoss side of a block
581 adjacent to the bedrock at the base of an ice mass will be complex and variable through space and
582 time (Hallet, 1979; Morland and Boulton, 1975; Ficker *et al*., 1980; Cohen *et al*., 2005). Yet, a simple
583 example below outlines the principles within the context of Shap granite erratics. Although a more
584 complex and complete appreciation of the stress environment of a boulder would be preferred, a
585 simple force balance is utilized instead. Simplicity is dictated by the absence of data to inform a more
586 complex model.

587

588 Setting the tensile stress at failure to 8 MPa and treating the rectangular block as subject to a critical
589 average driving force (τ_c) (Benn and Evans, 2011, p.114) due to ice flow, transverse and longitudinal
590 shear stresses arise of equal magnitude. Setting the fracture focus at half the block width in the
591 direction of loading, neglecting any water pressure variations (Cohen *et al*, 2006) and deformation
592 within a basal till (Hooke and Iverson, 1995), and imposing the driving stress transverse to the fracture

593 plane, as little as 180 m thickness (*H*) of flowing glacial ice with an ice surface slope (β) of 1.5° would
594 be sufficient to induce fracture in the block:
595
596 $$\tau_c = \rho_i \, g \, H \, tan \, \beta, \quad (3)$$
597
598 where ρ_i is the density of glacial ice and g is the acceleration due to gravity. The value of *H* = 180 m
599 pertains for a rectangular block with a surface area (*A*) defined by *L* = 2 m and *M* = 2 m (see
600 Supplementary Information section 1.7). The effective instantaneous stress might be greater than as
601 given by Equation 3 (Hooke and Iverson, 1995) but for a block with *L* = 3 m, *M* = 1 m with the long axis
602 transverse to the ice flow the shear force maximum might be achieved with only 130 m of ice cover
603 (see Supplementary Information section 1.7). To the east of the pluton the Last British Ice Sheet was
604 several hundred metres thick *c*., 25-22 ka BP (Evans *et al*., 2009), such that blocks would readily
605 fracture during full-glacial warm-based conditions where ice is flowing, as well as after the Last Glacial
606 Maximum when ice was thinning.
607
608 The smallest block sizes (*L* < *c*., 1.0 m) present in the field were not considered, which means that the
609 sampled population was truncated at the finer end. Nevertheless, although in some rock-types, a
610 lower limit to block strength may be related to a minimum structural block size (Dreimanis and
611 Vagners, 1971; Lim *et al*., 2004; Domokos *et al*., 2015) this is unlikely to pertain to granite which
612 breaks-down to grus at the scale of the phenocrysts. Nonetheless, fracture and surface wear, to an
613 initial block population, tend to result in the observed block population consisting of those blocks
614 which are strongly resistant to further comminution (Moss, 1972; Tavares and King, 1998; Larson and
615 Mooers, 2004; Pfeiffer *et al*., 2022) which, in principle, enables some blocks to survive transport
616 adjacent to the sole of the ice for great distances before being deposited during the waning phase of
617 the easterly directed ice stream (Hallet, 1979). Thus, although there may be no lower effective block
618 size, a statistical increase in resistance to fracture of the block population with distance likely is evident

as witnessed by the increased rounding seen in the Teesdale population. The occasional far-travelled large block, as noted in the Introduction, might be explained as being a statistically stronger example, in contrast to the remainder of the population. Alternatively, large blocks can be cushioned within the till body by smaller particles (Einav, 2007) thus avoiding fracture, or they can be transported englacially, rather than basally, and consequently not subject to protracted abrasion and significant compression whilst in traction. However, englacial blocks are more likely to be angular (Shilts, 1976; Boulton, 1978) and might retain rugose faces.

Thus, although the reduction in plume parameters values, such as block size and concentration, are commonly viewed as exponential functions of distance from the source (Shilts, 1976), such models (*e.g.*, Fig. 5) consider the sampled population as a whole and the inferences derived may not apply to the transport history of individual blocks. Certainly, the reduction in edge rounding for individual blocks is irregular with distance.

5 Conclusions

The hypothesis that granite blocks would display an increase in edge rounding with distance from the source outcrop is confirmed, whilst the hypothesis that shape would evolve with distance is refuted. Although the increase in the mean radius of edge rounding for the whole block population increases exponentially with distance, edge rounding on individual blocks is an irregular function mediated by block fracture mechanics, as block size reduces (with shapes fluctuating between cuboids, slabs and rods) with distance and new sharp edges are provided to partially edge-rounded blocks. Thus, edge rounding, and shape coevolve as block size is reduced. Fracture transverse to block orientation is in accord with the application of tensile stress which controls the process by which block form is conserved as block size is reduced. Consideration of the orientation of the tensile fractures on blocks in the field might be used to approximate the direction of ice flow at the time of fracture.

Overall, the results indicate that edge rounding is unlikely to be advanced if blocks continue to fracture. Well-rounded blocks must represent blocks that have resisted splitting. In the case of exceptionally large, rounded blocks, the rock mass likely is unusually homogeneous, lacking potential fracture lines. However, smaller blocks are less likely to contain potential fracture lines and so fracture should become less prevalent as blocks reduce in size, which then promotes edge rounding.

Future work should consider developing mathematical models that represent the function of edge rounding as predicated by a model (*e.g.*, silver ratio) describing block size reduction. Similar studies considering other lithologies (*e.g.*, stratified sedimentary rocks) likely would find different shape evolution patterns in contrast to the cuboid central tendency displayed by the homogeneous granite, with concomitant implications for edge rounding trends with time and distance.

Author contribution

PAC designed the study and conducted the field work, analysis, interpretation and drafting.

Competing interests

The author declares that he has no conflict of interest.

Acknowledgements

Emma Armstrong (Armstrongs Group) for access to the Shap (Pink) Quarry. Leslie Knight and David Evans (Durham University) provided information on the location of Shap granite erratics in Teesdale and near Levy Pool. Leslie Knight provided the base image for Fig. 3A. Two anonymous referees and

the editor, Arjen Stroeven, are thanked for their commentaries which led to improved presentation of the final results.

Data Availability

Basic data are available upon reasonable request from the author.

References

Anikoh, G.A., Adesida, P.A., Afolabi, O.C.: Investigation of physical and mechanical properties of selected rock types in Kogi State using hardness tests. *Journal of Mining World Express*, 4, 37-51. DOI:10.14355/mwe.2015.04.004, 2015.

Benn, D.I. : The genesis and significance of 'Hummocky Moraine': Evidence form the Isle of Skye, Scotland. *Quaternary Science Reviews*, 11, 781-799. https://doi.org/10.1016/0277-3791(92)90083-K, 1992.

Benn, D.I., Evans, D.J.A.: Glaciers and Glaciation, Hodder, London. 802pp, https://doi.org/10.1111/j.1502-3885.2011.00212.x, 2011.

Berger, A.R., Pitcher, W.S.: Structures in granitic rocks: A commentary and a critique on granite tectonics. *Proceedings of the Geological Association of London*, 81, 441–461. https://doi.org/10.1016/S0016-7878(70)80006-2, 1970.

Bouchard, M.A., Salonen, V.-P.: Block transport in shield areas, Glacial Indicator Trains, Kujansuu, R., Saarnisto, M., (editors), Balkema, Rotterdam, 87-107, ISBN 9781003079415, 1990.

Boulton, G.S.: Processes and patterns of glacial erosion. Glacial Geomorphology, Coates, D. R., editor), Binghamton, N.Y., State University of New York, 41-87, Publications in Geomorphology, ISBN: 9789401164931, 1974.

Boulton, G.S.: Boulder shapes and grain-size distributions of debris as indicators of transport paths through a glacier and till genesis. *Sedimentology*, 25, 773-799. https://doi.org/10.1111/J.1365-3091.1978.TB00329.X, 1978.

British Standard Institution: Code of Practice for Site Investigations, BS 5930 HMSO, London, 1981.

Buscarnera, G., Einav, I.: The mechanics of brittle granular materials with coevolving grain size and shape. *Proceedings of the Royal Society*, A, 477: 20201005. https://doi.org/10.1098/rspa.2020.1005, 2021.

Carling, P.A., Su, T., Meshkova, L.: Distribution of Devensian glacial erratics and related evidence elucidate complex ice flow changes across a former ice divide: Northern England. *Proceedings of the Geologists' Association*, 134, 139-165. https://doi.org/10.1016/j.pgeola.2023.01.002, 2023.

Caunt, S.L.: Igneous and Metamorphic Processes in the Shap Granite and its Aureole. Unpubl. PhD thesis, University of Leeds, 337pp, https://etheses.whiterose.ac.uk/522/, 1986.

Chiverrell, R.C., Thomas, G.S.P.: Extent and timing of the last glacial maximum (LGM) in Britain and Ireland: a review. *Journal of Quaternary Science*, 25, 535–549, 2010. https://doi.org/10.1002/jqs.1404

Clark, C.D., Ely, J.C., Hindmarsh, R.C.A., Bradley, S., Ignéczi, A., Fabel, D., Ó Cofaigh, C., Chiverrell, R.C., Scourse, J., Benetti, S., Bradwell, T., Evans, D.J.A., Roberts, D.H., Burke, M., Callard, S.L., Medialdea, A., Saher, M., Small, D., Smedley, R.K., Gasson, E., Gregoire, L., Gandy, N., Hughes, A.L.C., Ballantyne, C., Bateman, M.D., Bigg, G.R., Doole, J., Dove, D., Duller, G.A.T., Jenkins, G.T.H., Livingstone, S.L., McCarron, S., Moreton, S., Pollard, D., Praeg, D., Sejrup, H.P., van Landeghem, K.J.J., Wilson, P.: Growth and retreat of the last British–Irish Ice Sheet, 31 000 to 15 000 years ago: the BRITICE-CHRONOreconstruction. *Boreas*, 51, 1–60, 2022. https://doi.org/10.1111/bor.12594.

Clark, P.U., Dyke, A.S., Shakun, J.D., Carlson, A.E., Clark, J., Wohlfarth, B., Mitrovica, J.X., Hostetler, S.W., McCabe, M.: The Last Glacial Maximum. *Science*, 325, 710-714. https://doi.org/10.1126/science.1172873, 2009.

Cohen, D., Iverson, N.R., Hooyer, T.S., Fischer, U.H., Jackson, M., Moore, P.L.: Debris-bed friction of hard-bedded glaciers. *Journal of Geophysical Research*, 110, doi:10.1029/2004JF000228, 2005.

Cohen, D., Hooyer, T.S., Iverson, N.R., Thomason, J.F., Jackson, M.: Role of transient water pressure in quarrying: A subglacial experiment using acoustic emissions. J*ournal of Geophysical Research*, 111, F03006, doi:10.1029/2005JF000439, 2006.

Conroy, R.M., The RCSI Sample size handbook. Technical report, doi: 10.13140/RG.2.2.30497.51043 2018.

Daniel, W.W., Biostatistics: A Foundation for Analysis in the Health Sciences, 7th. New York, John Wiley and Sons, 1999.

Davies, B.J., Livingstone, S.J., Roberts, D.H., Evans, D.J.A., Gheorghiu, D.M., Ó Cofaigh, C.: Dynamic ice stream retreat in the central sector of the last British-Irish Ice Sheet. *Quaternary Science Reviews*, 225, 105989, 2019. https://doi.org/10.1016/j.quascirev.2019.105989

Day, M. J. and Goudie, A. S.: Field assessment of rock hardness using the Schmidt test hammer. *BGRG Technical Bulletin*, 18, 19-29. 1977.

Demirdag, S., Sengun, N., Ugur, I., Altindag, R.: Estimating the uniaxial compressive strength of rocks with Schmidt rebound hardness by considering the sample size. *Arabian Journal of Geosciences*, 11, 502, https://doi.org/10.1007/s12517-018-3847-1, 2018.

Domokos, G, Kun, F, Sipos, A.A., Szabó, T.: Universality of fragment shapes. *Scientific Reports,* 5, 9147. doi:10.1038/srep09147, 2015.

Dreimanis, A., Vagners, U.J.: Bimodal distributions of rock and mineral fragments in basal tills. Till: A Symposium, Goldthwait, R.P. (Editor), Ohio State University Press, Columbus, 237-250, ISBN 9780814201480 1971.

Einav, I.:) Breakage mechanics -Part 1: Theory. *Journal of Mechanics and Physics of Solids*, 55, 1274-1297. https://doi.org/10.1016/j.jmps.2006.11.003, 2007.

765 Engineering ToolBox: *Compression and Tension Strength of some Common Materials*. [online]
766 Available at: https://www.engineeringtoolbox.com/compression-tension-strength-d_1352.html,
767 2008 [Accessed 02 01 2023].

768 Evans, D.J.A.: Glacial erratics and till dispersal indicators. Encyclopaedia of Quaternary Science, S.A.
769 Elias (Editor), Elsevier, Oxford, 975-978, ISBN 978-0-444-52747-9, 2007.

770 Evans, D.J.A., Livingstone, S.J., Vieli, A., O´ Cofaigh, C.: The palaeoglaciology of the central sector of
771 the British and Irish Ice Sheet: reconciling glacial geomorphology and preliminary ice sheet
772 modelling. *Quaternary Science Reviews*, 28, 739-757. doi:10.1016/j.quascirev.2008.05.011, 2009.

773 Evans, D.J.A., Phillips, E.R., Hiemstra, J.F., Auton, C.: Subglacial till: Formation, sedimentary
774 characteristics and classification. *Earth-Science Reviews*, 78, 115-176,
775 doi:10.1016/j.earscirev.2006.04.001, 2006.

776 Firman, R. J.: Metamorphism and Metasomatism around the Shap and Eskdale granites, Durham
777 theses, Durham University. http://etheses.dur.ac.uk/9565/, 1953.

778 Ficker, F., Sonntag, G., Weber, E.: Asätze zur mechanischen deurung der rissentstehung bei
779 parablrissen und sichelbrűchen auf glaziageformten felsoberflächen. *Zeitshcrift fűr Gletscherkunde*
780 *und Glazialgeologie,* 16, 25-43, 1980.
781
782 Glasser, N.F.; Roman, M.; Holt, T.O.; Žebre, M.; Patton, H.; Hubbard, A.L.: Modification of bedrock
783 surfaces by glacial abrasion and quarrying: Evidence from North Wales. *Geomorphology*, 365,
784 107283. https://doi.org/10.1016/j.geomorph.2020.107283, 2020.
785
786 Goudie, A.S.: The Schmidt Hammer in geomorphological research. *Progress in Physical Geography*,
787 30, 703-718. https://doi.org/10.1177/0309133306071954, 2006.
788
789 Grantham, D.R.: The petrology of the Shap Granite. *Proceedings of the Geological Association*, 39,
790 299-331. https://doi.org/10.1016/S0016-7878(28)80015-0, 1928.
791
792 Hall, A.M., Krabbendam, M., van Boeckel, M., Goodfellow, B.W., Hättestrand, C., Heyman, J. et al.
793 (2020) Glacial ripping: geomorphological evidence from Sweden for a new process of glacial erosion.
794 Geografiska Annaler: Series A, Physical Geography, A102, 333–353.
795
796 Haldorsen, S.: Grain-size distribution of subglacial till and its relation to glacial crushing and abrasion.
797 *Boreas*, 10, 91-105. https://doi.org/10.1111/j.1502-3885.1981.tb00472.x, 1981.
798
799 Hallet, B.: A theoretical model of glacial abrasion. Journal of Glaciology, 23, 39-50.
800 https://doi.org/10.3189/S0022143000029725, 1979.
801
802 Hallet, B.: Glacial abrasion and sliding: Their dependence on the debris concentration in basal ice.
803 *Annals of Glaciology*, 2, 23–28. https://doi.org/10.3189/172756481794352487, 1981.
804
805 Hallet, B.: Glacial quarrying: a simple theoretical model. *Annals of Glaciology*, 22, 1-8.
806 https://doi.org/10.3189/1996AoG22-1-1-8, 1996.
807
808 Hiramatsu Y, Oka Y.: Determination of the tensile strength of rock by a compression test

of an irregular test piece. *International Journal of Rock Mechanics and Mining Sciences and Geomechanic Abstracts,* 3, 89–90. doi:10.1016/0148-9062(66)90002-7, 1966.

Hodgson, E.: The granite drift of Furness. *Geological Magazine*, 7, 328-339. https://doi.org/10.1017/S0016756800209801, 1870.

Hooke, R. LeB., Iverson, N.R.: Grain-size distribution in deforming subglacial tills: Role of grain fracture. *Geology*, 23, 57-60. https://doi.org/10.1130/0091-7613(1995)023%3C0057:GSDIDS%3E2.3.CO;2, 1995.

Holland, E.G.: Shap Granite. *Mine and Quarry Engineering*, 25, 2-15, 1959.

Hopkins, W.: On the transport of erratic blocks. *Transactions of the Cambridge Philosophical Society*, 8, 220-240, 1849.

Humlum, O.: Changes in texture and fabric of particles in glacial traction with distance from source, Myrdalsjokull, Iceland. *Journal of Glaciology,* 31 (108), 150-156. https://doi.org/10.3189/S0022143000006390, 1985.

Jahns, R. H.: Sheet structure in granites, its origin and use as a measure of glacial erosion in New England. *Journal of Geology*, 51, 71– 98, 1943.

Kirkbride, M.P.: Boulder edge-roundness as an indicator of relative age: A Lochnagar case study, *Scottish Geographical Journal*, 121, 219-236, https: doi: 10.1080/00369220518737232, 1985.

Kujansuu, R., Saarnisto, M.: Glacial Indicator Tracing, Balkema, Rotterdam, 252pp, ISBN 9781003079415, 1990.

Larson, P. C. and Mooers, H. D.: Glacial indicator dispersal processes: a conceptual model. *Boreas*, 33, 238–249. DOI 10.1080/03009480410001262, 2004.

Li, X.F., Li, H.B., Zhang, Q.B., Jiang, J.L., Zhao, J.: Dynamic fragmentation of rock material: Characteristic size, fragment distribution and pulverization law. *Engineering Fracture Mechanics*, 199, 739-759. https://doi.org/10.1016/j.engfracmech.2018.06.024, 2018.

Lim, W.L., McDowell, G.R., Collop, A.C.: The application of Weibull statistics to the strength of railway ballast. *Granular Matter*, 6, 229–237. http://dx.doi.org/10.1007/s10035-004-0180-z, 2004.

Lliboutry, L.L.: Monolithologic erosion of hard beds by temperate glaciers. *Journal of Glaciology*, 40, 433-450. https://doi.org/10.3189/S0022143000012314, 1994.

Livingstone, S.J., Evans, D.J.A., Ó Cofaigh, C., Davies, B.J., Merritt, J.W., Huddart, D., Mitchell, W.A., Roberts, D.H., Yorke, L.: Glaciodynamics of the central sector of the last British-Irish Ice Sheet in Northern England. *Earth-Science Reviews*, 111, 25-55. https://doi.org/10.1016/j.earscirev.2011.12.006, 2012.

MacGregor, K., Anderson, R.S., Waddington, E.D.: Numerical modeling of glacial erosion and headwall processes in alpine valleys. *Geomorphology*, 103, 189–204. https://doi.org/10.1016/j.geomorph.2008.04.022, 2009.

Man, K., Wang, K., Liu, X.: Dynamic tensile properties of granite varied with depths under a similar loading rate. *Advances in Civil Engineering*, Article ID 6048312, https://doi.org/10.1155/2018/6048312, 2018.

Matthes, F. E.: Geological history of the Yosemite Valley. U.S. Geological Survey. Professional Paper 160, 160pp, 1930.

Merritt, J.W., Hall, A.M., Gordon, J.E., Connel, E.R.: Late Pleistocene sediments, landforms and events in Scotland: a review of the terrestrial stratigraphic record. *Earth and Environmental Science Transactions of the Royal Society of Edinburgh*, 110, 39-91. https://doi.org/10.1017/S1755691018000890, 2019.

Morland, L.W., Boulton, G.S.: Stress in an elastic hump: the effects of glacier flow over elastic bedrock. *Proceedings of the Royal Society*, *A,* 344, 157-173. https://doi.org/10.1098/rspa.1975.0096, 1975.

Moss, A.J.: Technique for assessment of blocks breakage in natural and artificial environments. *Journal of Sedimentary Petrology*, 42, 725–728. https://doi.org/10.1306/74D7261C-2B21-11D7-8648000102C1865D, 1972.

Nicholson, H.A.: On the granite of Shap, in Westmoreland. *Transactions of the Edinburgh Geological Society,* 1, 133-37, https://doi.org/10.1144/transed.1.2.133, 1868.

Oakey, R.J., Green, M., Carling, P.A., Lee, M.W.E., Sear, D.A., Warburton, J.: Grain-shape analysis– A new method for determining representative blocks shapes for populations of natural grains. *Journal of Sedimentary Research*, 75, 1065-1073. https://doi.org/10.2110/jsr.2005.079, 2005.

Olsen, L.: A method for determining total block roundness in sediments. *Boreas*, 12, 17-21. http://dx.doi.org/10.1111/j.1502-3885.1983.tb00355.x, 1983.

Pfeiffer, A. M., Morey, S., Karlsson, H. M., Fordham, E. M., and Montgomery, D. R.: Survival of the strong and dense: Field evidence for rapid, transport-dependent bed material abrasion of heterogeneous source lithology. *Journal of Geophysical Research: Earth Surface*, 127, e2021JF006455. https://doi.org/10.1029/2021JF006455, 2022.

Parsons I., Lee, M.R.: Minerals are not just chemical compounds. *The Canadian Mineralogist*, 43, 1959-1992. https://doi.org/10.2113/gscanmin.43.6.1959, 2005.

Rose, J.: The Dimlington Stadial/Dimlington Chronozone: a proposal for naming the main glacial episode of the Late Devensian in Britain. *Boreas*, 14, 225–230, 1985. https://doi.org/10.1111/j.1502-3885.1985.tb00724.x

Scourse, J.D., Haapaniemi, A.I., Colmenero-Hidalgo, E., Peck, V.L., Hall, I.R., Austin, W.E.N., Knutz, P.C., Zahn, R.: Growth, dynamics and deglaciation of the last British–Irish ice sheet: the deep-sea ice-rafted detritus record. *Quaternary Science Reviews* 28, 3066–3084, 2009.Seo, D., Sohn, C., Cil, M.B., Buscarnera, G.: Evolution of blocks morphology and mode of fracture during the oedometric compression of sand. *Géotechnique*, 71, 853-865. https://doi.org/10.1680/jgeot.18.P.300, 2021.

Shilts, W.W.: Glacial till and mineral exploration. Glacial Till, An Interdisciplinary Study, R.F. Legget (editor), Royal Society of Canada, Special Publication, 12, 205-224, https://doi.org/10.2136/sssaj1977.03615995004100010004x, 1976.

Shipway P, Hutchings I.: Fracture of brittle spheres under compression and impact loading. I. Elastic stress distributions. *Philosophical Magazine, A* **67**, 1389–1404. https://doi.org/10.1080/01418619308225362, 1993.

Tavares, L.M., King, R.P.: Single-blocks fracture under impact loading. *International Journal of Mineral Processing*, 54, 1–28. https://doi.org/10.1016/S0301-7516(98)00005-2, 1998.

Ugelvig, S. V., Egholm, D.L., Iverson, N.R.: Glacial landscape evolution by subglacial quarrying: A multiscale computational approach. *Journal of Geophysical Research: Earth Surface*, 121, doi:10.1002/2016JF003960, 2016.

Wager, L.R.: A stage in the decomposition of biotite from the Shap Granite. *Proceedings of the Yorkshire Geological Society*, 25, 366-342, 1944.

Wang, X.-Y., Yin, Y.-C., Xing, M.-L., Zhang, D.-D., Chen, Y., Wang, E.-C.: Microsimulation study on energy release and rock block ejection force of granite under different unloading conditions. *Frontiers in Earth Science*, 10:909371. doi: 10.3389/feart.2022.909371, 2022.

Wentworth, C.K.: A method of measuring and plotting the shapes of pebbles. *US Geological Society Bulletin* 730-C, 91-102. doi: 10.3133/B730C, 1923.

Westaway, R.: Quaternary uplift of northern England. *Global and Planetary Change*, 68, 357-382. https://doi.org/10.1016/j.gloplacha.2009.03.005, 2009.

Yu, M., Wei, C., Niu, L., Li, S., Yu, Y.: Calculation for tensile strength and fracture toughness of granite with three kinds of grain sizes using three-point-bending test. *PLoS ONE*, 13, e0180880. https://doi.org/10.1371/journal. pone.0180880, 2018.

Zingg, T.: Beitrag zur schotteranalyse: Die Schotteranalyse und ihre Anwendung auf die Glattalschotter. PhD thesis, ETH Zurich. https://www.reasher-collection.ethz.ch/handle/20.500.11850/135183, 1935.